Covariance Statistics of Polarimetric Brightness Temperature Measurements

Jinzheng Peng and Christopher S. Ruf, *Fellow, IEEE*

***Abstract*—All microwave radiometer measurements of brightness temperature (T_B) include an additive noise component. With conventional linearly polarized radiometers, the variance of the noise is a well-understood function of the system temperature, the predetection bandwidth, and the integration time according to the so-called "radiometer uncertainty equation." The noise has generally been considered to be uncorrelated between orthogonally polarized channels. The variance and the correlation statistics of the additive noise component of fully polarimetric radiometer measurements are derived from theoretical considerations, and the resulting relationships are experimentally verified. It is found that the noise can be correlated between polarimetric channels, and the correlation statistics will vary as a function of the polarization state of the scene under observation. For example, a strong correlation is typical between the noise in either vertically or horizontally polarized T_B and the 45° slant linear polarizations that are often used to derive the third Stokes T_B. A weak, but nonzero, correlation is also possible between the additive noise in the vertically and horizontally polarized T_B's themselves. This is a correction to the common assumption that they are uncorrelated.**

***Index Terms*—Microwave radiometry, noise statistics, polarimetric radiometry.**

I. Introduction

A MICROWAVE radiometer's measurement of the brightness temperature (T_B) is an estimate of the variance of a random thermal emission signal derived from samples of the signal. Because the number of samples is always finite, the estimate is itself a random signal. The standard deviation of the estimate is given by the "radiometer uncertainty equation" $\Delta T = KT_{\rm sys}/\sqrt{B\tau}$, where K is an instrument-specific constant, $T_{\rm sys}$ is the system noise temperature of the radiometer, B is its predetection bandwidth, and τ is the integration time of the measurement [1]. The "ΔT" of a radiometer measurement is of fundamental importance and often determines the precision with which geophysical parameters of interest can be estimated from measurements of T_B. In most cases, geophysical parameter retrievals are derived from two or more radiometer measurements made at different polarizations and/or frequencies. The uncertainty in the retrieval due to ΔT noise will depend on the variance of the noise and on the covariance between the different measurements. Measurements made at different frequencies will, in most cases, have uncorrelated noise because the signals originate from different portions of the electromagnetic spectrum and are processed by different channels of the radiometer hardware. Measurements of different polarization components at the same frequency are made by processing the thermal emission signal through some common and some different stages of the radiometer hardware. The covariance statistics of these measurements are the subject of this paper.

The most common nonfully polarimetric radiometers measure two orthogonal linear polarization components of the thermal emission signal using separate receivers connected to a single antenna with an orthomode transducer that separates the two desired polarization components apart. The receivers estimate the variance of the signal by performing a time average of the square of the signal. The two resulting components of T_B are designated T_v and T_h for vertical and horizontal polarizations, respectively. Two common types of fully polarimetric radiometers are used to measure the complete Stokes parameters of the signal based on either incoherent or coherent detection [2]. An incoherent detection radiometer measures the variance of certain polarimetric components of the signal—most often, the $\pm 45^\circ$ slant linear and left- and right-hand circular polarizations—in addition to the vertical and horizontal polarizations. The additional components of T_B are designated T_P, T_M, T_L, and T_R for $+45^\circ$ and -45° slant linear and left- and right-hand circular polarizations, respectively. This is the approach used by the spaceborne WindSat radiometer [3], whose polarimetric capabilities have proven to be effective at estimating the ocean surface wind direction [4], [5]. The variance and, hence, the T_B of each component can be estimated using the same squaring and time-averaging signal processing steps as are used in the nonpolarimetric case. The additional polarization components of the thermal emission signal can be generated in a number of ways. The most common approach uses hybrid combiners, which add together the vertically and horizontally polarized components with relative phase differences of $0^\circ, \pm 90^\circ$, and 180° [6], [7]. Quasi-optical methods have also been employed to generate the desired polarizations [8]. A coherent detection radiometer directly measures the complex correlation between the vertical and horizontal polarization components of the signal. The correlation operation requires signal multiplication and integration processing. Early versions of correlators, based on analog electronics, were commonly used in radio astronomy [9]. A more modern implementation estimates the correlation by digitizing the vertical and horizontal polarization components of the signal and then multiplying and averaging (i.e., correlating) them

Manuscript received July 31, 2007; revised March 15, 2008. Current version published October 1, 2008. This work was supported in part by the National Aeronautics and Space Administration under Grant NNG04HZ28C.

The authors are with Space Physics Research Laboratory, University of Michigan, Ann Arbor, MI 48109-2143 USA (e-mail: cruf@umich.edu).

Color versions of one or more of the figures in this paper are available online at http://ieeexplore.ieee.org.

Digital Object Identifier 10.1109/TGRS.2008.921413

in a digital signal processor [10]. The resulting components of T_B are designated T_3 and T_4 for the real and imaginary components of the correlation, respectively. This approach will be used by the upcoming Soil Moisture and Ocean Salinity spaceborne radiometer [11].

If the vertically and horizontally polarized components of the electric field radiated by thermal emission are designated as E_V and E_H, respectively, then the polarimetric components of T_B can be expressed as:

$$T_v = c\left\langle |E_V|^2 \right\rangle \qquad T_h = c\left\langle |E_H|^2 \right\rangle \tag{1a}$$

$$T_P = c\left\langle \left| \frac{E_V + E_H}{\sqrt{2}} \right|^2 \right\rangle \qquad T_M = c\left\langle \left| \frac{E_V - E_H}{\sqrt{2}} \right|^2 \right\rangle \tag{1b}$$

$$T_L = c\left\langle \left| \frac{E_H - jE_V}{\sqrt{2}} \right|^2 \right\rangle \qquad T_R = c\left\langle \left| \frac{E_H + jE_V}{\sqrt{2}} \right|^2 \right\rangle \tag{1c}$$

$$T_3 = 2c\mathrm{Re}\left\{\langle |E_V E_H^*| \rangle\right\} \qquad T_4 = 2c\mathrm{Im}\left\{\langle |E_V E_H^*| \rangle\right\} \tag{1d}$$

$c = \lambda^2/k\eta B$, where λ is the signal wavelength, k is the Boltzmann constant, η is the intrinsic impedance of free space, and B is the signal bandwidth. Relationships between the various components follow from (1) as [10]:

$$T_P = \frac{T_v + T_h + T_3}{2} \qquad T_M = \frac{T_v + T_h - T_3}{2} \tag{2a}$$

$$T_L = \frac{T_v + T_h + T_4}{2} \qquad T_R = \frac{T_v + T_h - T_4}{2} \tag{2b}$$

$$T_3 = T_P - T_M \quad \text{or} \quad T_3 = 2T_P - T_v - T_h \quad \text{or} \quad T_3 = T_v + T_h - 2T_M \tag{2c}$$

$$T_4 = T_L - T_R \quad \text{or} \quad T_4 = 2T_L - T_v - T_h \quad \text{or} \quad T_4 = T_v + T_h - 2T_R. \tag{2d}$$

Equations (2c) and (2d) represent the algorithms by which the third and fourth Stokes parameters are typically derived with an incoherent detection fully polarimetric radiometer. Note that, in each case, there are three options to choose from. The second and third options require one less receiver to implement than the first and, therefore, would seem to be the more cost-effective approaches. However, in practice, the first option is almost exclusively used because it is much better able to reject common mode calibration biases that are present in the incoherent detection channels. The other two options might be used as backup algorithms in case of a radiometer hardware failure.

In the following sections, the complete covariance matrix is developed for measurements of fully polarimetric T_B using the incoherent and coherent detection methods. From the covariance, the "ΔT" noise associated with each individual polarization component is derived. Expressions for the degree of correlation between the "ΔT" noise in each component are also derived. Given the complete covariance behavior of the T_B components, the variance of arbitrary algebraic combinations can be derived. The dependence of the covariance on the polarization state of the signal is illustrated by an example that considers the variance of measurements of T_3 that would result from using the incoherent detection approach and each of the three algorithms in (2c). Last, experimental confirmation of the results is presented by comparing the predicted and measured correlations between the "ΔT" noise in the measurements of T_v, T_h, and T_3 using a coherent detection radiometer.

II. Noise Covariance of an Incoherent Detection Hybrid-Combining Polarimetric Radiometer

The signal flow through a hybrid-combining polarimetric microwave radiometer is diagrammed in Fig. 1. In the figure, G_v and G_h represent the gains of the V- and H-pol channels, respectively, B is their bandwidth (assumed the same in each channel), and $v_v(t)$ and $v_h(t)$ are the amplified and filtered signal voltages from the V- and H-pol channels, respectively. These two signals can be written as the sum of an external component, originating from the observed scene, and an internal component, originating from the noise in the receiver electronics, or

$$\begin{aligned} v_v(t) &= \sqrt{G_v}\,[b_v(t) + n_v(t)] \\ v_h(t) &= \sqrt{G_h}\,[b_h(t) + n_h(t)] \end{aligned} \tag{3}$$

where $b_v(t)$ and $b_h(t)$ are the time-varying noise voltages associated with the brightness temperature (see [12] for a detailed definition), and $n_v(t)$ and $n_h(t)$ are the time-varying noise voltages associated with the receiver noise in the V- and H-pol channels, respectively. The noise voltages $b_v(t)$ and $b_h(t)$ are the scaled versions of the incident electric field, with units of $K^{-1/2}$. Both $b(t)$ and $n(t)$ are additive zero-mean band-limited Gaussian-distributed random variables. The autocorrelation and cross-correlation relationships between the voltages associated with the brightness temperatures are given by [12]

$$\langle b_v(t) b_v(t-\tau)\rangle = T_v \cos(2\pi f_c \tau)\mathrm{sinc}(B\tau) \tag{4a}$$

$$\langle b_h(t) b_h(t-\tau)\rangle = T_h \cos(2\pi f_c \tau)\mathrm{sinc}(B\tau) \tag{4b}$$

$$\langle b_v(t) b_h(t-\tau)\rangle = \left\{\frac{T_3}{2}\cos(2\pi f_c \tau) - \frac{T_4}{2}\sin(2\pi f_c \tau)\right\}\mathrm{sinc}(B\tau) \tag{4c}$$

where T_v and T_h are the V- and H-pol brightness temperatures, respectively, f_c is the center frequency of the signal, B is its bandwidth, and $\mathrm{sinc}(u) = \sin(\pi u)/(\pi u)$. The variance and the covariance of the signals are found by evaluating these autocorrelations at $\tau = 0$, or

$$\left\langle b_v^2(t)\right\rangle = T_v \tag{5a}$$

$$\left\langle b_h^2(t)\right\rangle = T_h \tag{5b}$$

$$2\left\langle b_v(t) b_h(t)\right\rangle = T_3. \tag{5c}$$

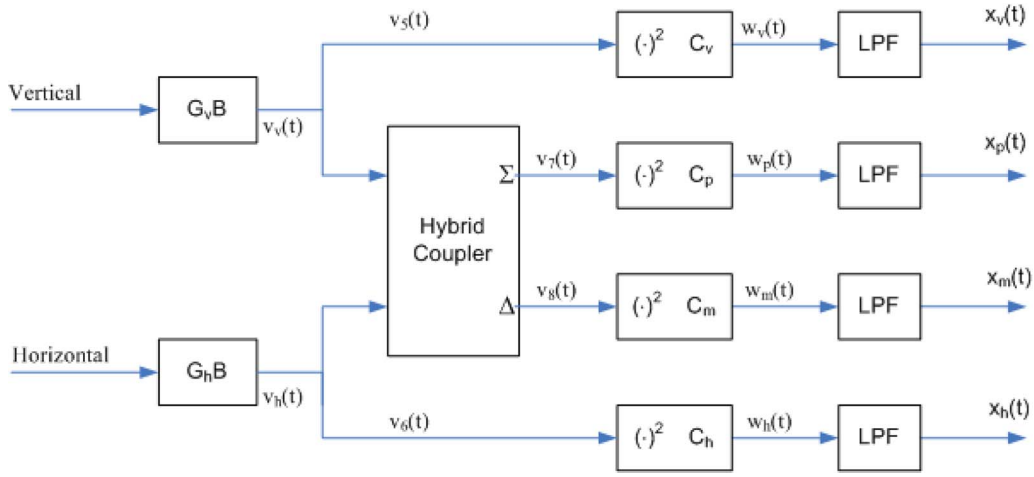

Fig. 1. Signal flow diagram for a hybrid-combining polarimetric microwave radiometer.

The variance of $n(t)$ is similarly related to the receiver noise temperature by

$$\left\langle n_v^2(t)\right\rangle = T_{Rv} \qquad \left\langle n_h^2(t)\right\rangle = T_{Rh} \tag{6}$$

where T_{Rv} and T_{Rh} are the noise temperatures of the V- and H-pol receivers, respectively. The receiver noise is uncorrelated between channels, so that

$$\langle n_v(t) n_h(t)\rangle = 0. \tag{7}$$

A hybrid-combining polarimetric radiometer forms $\pm 45^\circ$ slant linearly polarized channels from $v_v(t)$ and $v_h(t)$ by summing and subtracting them in a hybrid coupler, as shown in Fig. 1. The signals $v_v(t)$ and $v_h(t)$ are first split into two channels, or

$$v_5(t) = \frac{v_v(t)}{\sqrt{2}} \tag{8a}$$

$$v_6(t) = \frac{v_h(t)}{\sqrt{2}}. \tag{8b}$$

The hybrid coupler then adds and subtracts them to produce the slant linear signals, or

$$v_7(t) = \frac{v_v(t) + v_h(t)}{2} \tag{9a}$$

$$v_8(t) = \frac{v_v(t) - v_h(t)}{2}. \tag{9b}$$

The output signals from the hybrid as well as the original signals are then passed through square-law detectors. Their outputs are given by

$$w_v(t) = \frac{c_v}{2} v_v^2(t) \tag{10a}$$

$$w_p(t) = \frac{c_p}{4} \left[v_v(t) + v_h(t)\right]^2 \tag{10b}$$

$$w_m(t) = \frac{c_m}{4} \left[v_v(t) - v_h(t)\right]^2 \tag{10c}$$

$$w_h(t) = \frac{c_h}{2} v_h^2(t) \tag{10d}$$

where c_x is the detector sensitivity for polarization channel $x = v$, p, m, and h. Last, the four signals are integrated and sampled. The integration process is modeled as an ideal low-pass filter (LPF in Fig. 1). The low-pass-filtered versions of the four polarization signals are $x_v(t)$, $x_p(t)$, $x_m(t)$, and $x_h(t)$, respectively. The expected values of these signals (i.e., the dc component of their spectra) are proportional to the four associated brightness temperatures. The variance of the signals (i.e., the integral over the ac components of their spectra) represents the additive noise present in the measurements.

The autocorrelations and cross correlations, and the spectra and cross spectra of the four low-pass-filtered signals, i.e., $x_v(t)$, $x_p(t)$, $x_m(t)$, and $x_h(t)$, are derived in Appendix A. From these, it is possible to compute their covariance and related statistics. The correlation between $x_v(t)$ and $x_p(t)$ can be expressed as follows:

$$\rho_{v,p} = \frac{\langle (x_v(t) - \langle x_v(t)\rangle)\,(x_p(t) - \langle x_p(t)\rangle)\rangle}{\sqrt{\mathrm{Var}(x_v(t))}\cdot\sqrt{\mathrm{Var}(x_p(t))}} = \frac{\left[(T_v + T_{Rv}) + \frac{\sqrt{g}}{2} T_3\right]^2 + \frac{g}{4} T_4^2}{(T_v + T_{Rv})\cdot\left\{(T_v + T_{Rv}) + g(T_h + T_{Rv}) + \sqrt{g} T_3\right\}} \tag{11a}$$

where $g = G_h/G_v$ is the ratio of H- to V-pol channel gains. Similarly, for the correlation between polarization pairs $v\&m$, $p\&m$, $p\&h$, and $m\&h$, we have (11b)–(11f), shown at the bottom of the next page. Note that the correlation coefficients are independent of the bandwidth B and the integration time τ.

The ΔT of each channel is given by

$$\Delta T_v = \frac{T_{\mathrm{sys},v}}{\sqrt{B\tau}} = \frac{T_v + T_{Rv}}{\sqrt{B\tau}} \tag{12a}$$

$$\Delta T_p = \frac{T_{\mathrm{sys},p}}{\sqrt{B\tau}} = \frac{1}{\sqrt{B\tau}} \cdot \frac{(T_v + T_{Rv}) + g(T_h + T_{Rh}) + \sqrt{g} T_3}{2\sqrt{g}} \tag{12b}$$

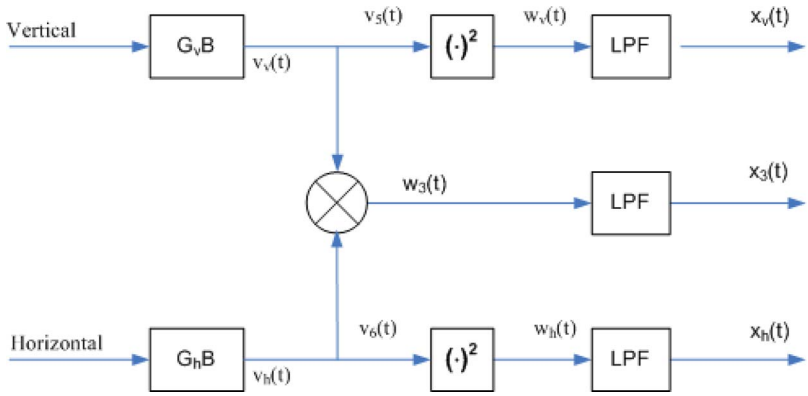

Fig. 2. Signal flow diagram for a correlating polarimetric microwave radiometer.

$$\Delta T_m = \frac{T_{\mathrm{sys},m}}{\sqrt{B\tau}} = \frac{1}{\sqrt{B\tau}} \cdot \frac{(T_v + T_{Rv}) + g(T_h + T_{Rh}) - \sqrt{g}T_3}{2\sqrt{g}} \tag{12c}$$

$$\Delta T_h = \frac{T_{\mathrm{sys},h}}{\sqrt{B\tau}} = \frac{T_h + T_{Rh}}{\sqrt{B\tau}}. \tag{12d}$$

III. Noise Covariance of a Coherent Detection Correlating Polarimetric Radiometer

The signal flow through a correlating polarimetric radiometer is shown in Fig. 2. The voltage signals $v_v(t)-v_6(t)$ and their correlation statistics are identical to those associated with the hybrid-combining radiometer analysis given in Section II, as are the two low-pass-filtered signals $x_v(t)$ and $x_h(t)$ for the vertically and horizontally polarized channels, respectively. The signal in the cross-correlating channel of the radiometer, prior to low-pass filtering, is given by

$$w_3(t) = v_v(t) \cdot v_h(t). \tag{13}$$

After the low-pass filter, the correlating channel signal becomes $x_3(t)$.

The procedure that followed to derive the covariance relationships between the three low-pass-filtered signals is similar to that for the hybrid-combining radiometer. Details are presented in Appendix B. The correlation coefficient between the outputs $x_v(t)$ and $x_3(t)$ can be expressed as follows:

$$\rho_{v,3} = \frac{R^{\mathrm{ac}}_{v,3}(t)}{\sqrt{R^{\mathrm{ac}}_{v,v}(t)} \cdot \sqrt{R^{\mathrm{ac}}_{3,3}(t)}} = \frac{\sqrt{2}T_3}{\sqrt{4(T_v + T_{Rv})(T_h + T_{Rh}) + \{T_3^2 - T_4^2\}}}. \tag{14a}$$

Similarly, for the other channel pairs, we have

$$\rho_{v,h} = \frac{T_3^2 + T_4^2}{4(T_v + T_{Rv})(T_h + T_{Rh})} \tag{14b}$$

$$\rho_{h,3} = \frac{\sqrt{2}T_3}{\sqrt{4(T_v + T_{Rv})(T_h + T_{Rh}) + \{T_3^2 - T_4^2\}}}. \tag{14c}$$

$$\rho_{v,m} = \frac{\left[(T_v + T_{Rv}) - \frac{\sqrt{g}}{2}T_3\right]^2 + \frac{g}{4}T_4^2}{(T_v + T_{Rv}) \cdot \left\{(T_v + T_{Rv}) + g(T_h + T_{Rv}) - \sqrt{g}T_3\right\}} \tag{11b}$$

$$\rho_{v,h} = \frac{T_3^2 + T_4^2}{4(T_v + T_{Rv})(T_h + T_{Rh})} \tag{11c}$$

$$\rho_{p,m} = \frac{[(T_v + T_{Rv}) - g(T_h + T_{Rh})]^2 + gT_4^2}{\left\{(T_v + T_{Rv}) + g(T_h + T_{Rh}) + \sqrt{g}T_3\right\} \cdot \left\{(T_v + T_{Rv}) + g(T_h + T_{Rh}) - \sqrt{g}T_3\right\}} \tag{11d}$$

$$\rho_{p,h} = \frac{\left[g(T_h + T_{Rh}) + \frac{\sqrt{g}}{2}T_3\right]^2 + \frac{g}{4}T_4^2}{g(T_h + T_{Rh}) \cdot \left\{(T_v + T_{Rv}) + g(T_h + T_{Rh}) + \sqrt{g}T_3\right\}} \tag{11e}$$

$$\rho_{m,h} = \frac{\left[g(T_h + T_{Rh}) - \frac{\sqrt{g}}{2}T_3\right]^2 + \frac{g}{4}T_4^2}{g(T_h + T_{Rh}) \cdot \left\{(T_v + T_{Rv}) + g(T_h + T_{Rh}) - \sqrt{g}T_3\right\}} \tag{11f}$$

The NEΔT of each channel is given by

$$\Delta T_v = \frac{T_v + T_{Rv}}{\sqrt{B\tau}} \tag{15a}$$

$$\Delta T_3 = \frac{\sqrt{2(T_v + T_{Rv})(T_h + T_{Rh}) + 0.5\,(T_3^2 - T_4^2)}}{\sqrt{B\tau}} \tag{15b}$$

$$\Delta T_h = \frac{T_h + T_{Rh}}{\sqrt{B\tau}}. \tag{15c}$$

IV. Application—The Third Stokes T_B With a Hybrid-Combining Radiometer

There are three methods to obtain the third Stokes brightness temperature from the measurements made by a hybrid-combining polarimetric radiometer. The three methods, denoted as $T_{3.1}$, $T_{3.2}$, and $T_{3.3}$, are given by

$$\begin{aligned} T_{3.1} &= T_p - T_m \\ &= [\,0 \quad 1 \quad -1 \quad 0\,] \cdot [\,T_v \quad T_p \quad T_m \quad T_h\,]^t \end{aligned} \tag{16a}$$

$$\begin{aligned} T_{3.2} &= 2T_p - T_v - T_h \\ &= [\,-1 \quad 2 \quad 0 \quad -1\,] \cdot [\,T_v \quad T_p \quad T_m \quad T_h\,]^t \end{aligned} \tag{16b}$$

$$\begin{aligned} T_{3.3} &= T_v + T_h - 2T_m \\ &= [\,1 \quad 0 \quad -2 \quad 1\,] \cdot [\,T_v \quad T_p \quad T_m \quad T_h\,]^t \end{aligned} \tag{16c}$$

where T_v, T_p, T_m, and T_h are the measured brightness temperatures. For each of these methods, the variance of T_3 can be obtained using the error propagator, i.e.,

$$\Lambda_{T3} = A \cdot \Lambda_T \cdot A^t \tag{17}$$

where A, the 1×4 matrix satisfying $T_3 = A \cdot T$, is given in (16) for each method, and where $T = [T_v \quad T_p \quad T_m \quad T_h]^t$ is the random vector with covariance matrix Λ_T. Λ_T, the covariance matrix for the signals $x_v(t)$, $x_p(t)$, $x_m(t)$, and $x_h(t)$, can be expressed as follows:

$$\Lambda_T = \begin{bmatrix} R^{\rm ac}_{v,v}(0) & R^{\rm ac}_{v,p}(0) & R^{\rm ac}_{v,m}(0) & R^{\rm ac}_{v,h}(0) \\ R^{\rm ac}_{p,v}(0) & R^{\rm ac}_{p,p}(0) & R^{\rm ac}_{p,m}(0) & R^{\rm ac}_{p,h}(0) \\ R^{\rm ac}_{m,v}(0) & R^{\rm ac}_{m,p}(0) & R^{\rm ac}_{m,m}(0) & R^{\rm ac}_{m,h}(0) \\ R^{\rm ac}_{h,v}(0) & R^{\rm ac}_{h,p}(0) & R^{\rm ac}_{h,m}(0) & R^{\rm ac}_{h,h}(0) \end{bmatrix} \tag{18}$$

where $R^{\rm ac}_{a,b}(0)$ denotes the variance of $a(t)$ if $a(t) = b(t)$ or the covariance of $a(t)$ with $b(t)$ if $a(t) \neq b(t)$. See Section II and Appendix A for expressions for these variance and covariance elements. If these expressions are substituted into (18), the covariance matrix can be obtained. Combining (16) and (18) for each of the three methods results in individual covariance matrices for each of the three methods that are given by (19a)–(19c), shown at the bottom of the next page.

If all detector sensitivities are assumed to be the same (i.e., if $c_v = c_p = c_m = c_h$), then the variance of each version of T_3 is also the same. This might, at first, seem counterintuitive. For example, if the additive noise in the measurements of T_v, T_h, T_p, and T_m had been uncorrelated, then the variance of $T_{3.1}$ $(= T_p - T_m)$ would have been double that of either T_p or T_m, whereas the variance of both $T_{3.2}$ $(= 2T_p - T_v - T_h)$ and $T_{3.3}$ $(= -2T_m + T_v + T_h)$ would have been four times as large. In fact, the partial correlation between the additive noise in T_v, T_h, T_p, and T_m precisely compensates, so that the variances for all methods are equal. For the case of $c_v = c_p = c_m = c_h = 1$, the standard deviation of the additive noise in T_3 (using any of the three methods) is given by

$$\Delta T_3 = \sqrt{\frac{4(T_v + T_{Rv})(T_h + T_{Rh}) + (T_3^2 - T_4^2)}{2B\tau}}. \tag{20}$$

In most cases, (20) could be used as a convenient "working equation" for predicting the precision of the measurements of T_3.

V. Experimental Verification of Covariance Relationships

Some of the noise correlation statistics derived above have been experimentally evaluated. A bench top L-band radiometer was used, which has separate vertical and horizontal linear polarization input channels, followed by standard amplification, down-conversion, and square-law detection stages for the two channels plus a third channel that digitizes the two signals, multiplies them together, and averages the product. Thus, this is a coherent detection radiometer of the type described in Section III, which can measure T_v, T_h, and T_3. Signals entering the V- and H-pol input ports of the radiometer were generated using the correlated noise calibration standard (CNCS). CNCS is a programmable polarimetric calibration target that is capable of generating pairs of thermal noise signals with adjustable and repeatable relative correlation statistics [13]–[15]. The dynamic range of brightness temperatures that can be generated by the CNCS is approximately 90–400 K for T_v and T_h and -550 to $+550$ K for T_3 and T_4. For purposes of this experiment, stable 90- and 310-K T_B's were generated at both V- and H-pol as calibration references for the radiometer. The calibration signals were uncorrelated $(T_3 = T_4 = 0)$. Interleaved between the calibration signals were signals for which $T_v = T_h = 400$ K, and the partial correlation between T_v and T_h was adjusted so that T_3 varied between 0 and 550 K in ten uniformly spaced steps. Because the radiometer does not measure T_4, the quadrature component of the correlation between V- and H-pol signals was set to zero.

For each value of T_3, an extended time series of measurements of T_v, T_h, and T_3 was simultaneously recorded. From these measurements, correlation coefficients between the additive noise in each channel can be derived. This process was repeated three times as a means of determining the standard error and the repeatability of the estimates of the correlation coefficient statistic. The results are shown in Fig. 3(a)–(c), which respectively plot the average and the standard deviation of the correlation between the noise in T_v and T_3, T_h and T_3, and T_v and T_h as a function of T_3. The correlation values that are predicted by theory are also plotted for comparison. The predicted and measured correlations in Fig. 3(a) and (b) closely agree, with the correlation monotonically rising as a function of T_3. This behavior is what produced the similar values for the ΔT of T_3 noted in Section IV, regardless of which of the

three methods was used to derive it from hybrid-combining radiometer measurements. In Fig. 3(c), both the predicted and measured correlations between noise in T_v and T_h are quite low but can be seen to slightly increase at the higher values of T_3. Even at the highest values of T_3, however, such a small level of correlation would, in most practical applications, not be a concern.

The higher values of the measured correlation between T_v and T_h, relative to the theoretical predictions, are probably due to limitations in the means by which the test signals were generated. The partially correlated test signals were generated using a commercial arbitrary waveform generator containing a pair of lookup tables with 262 114 12-bit integer entries, which are used to simulate the random noise signals. The limited size and bit length of the pseudorandom test signals impose an additional degree of correlation on the measurements above that of ideal random sequences of infinite length and precision.

VI. Conclusion

General expressions have been developed for the covariance of the additive noise present in the measurements of the polarimetric components of the brightness temperature. The standard vertical and horizontal linearly polarized components are considered, as well as the most common fully polarimetric components—$\pm 45^\circ$ slant linear and left- and right-hand circular—and direct measurements of the third and fourth Stokes parameters by a coherent detection radiometer. The NEΔT of individual polarimetric components are given by the square root of the main diagonal of the covariance matrix. The off-diagonal elements of the covariance matrix can be used to derive the correlation between noise in different polarimetric components. Knowledge of the complete covariance matrix also permits the computation of the noise present in arbitrary linear combinations of the components. This was demonstrated by examining the noise associated with three different methods for deriving the third Stokes parameter from vertical, horizontal, and $\pm 45^\circ$ slant linear polarization measurements. The covariance matrix can also be used to determine the noise associated with other linear combinations of the brightness temperatures, such as are often a part of geophysical retrieval algorithms.

Appendix A
Covariance of Hybrid-Combining Polarimetric Radiometer Signals

The time-varying voltages $b_v(t)$ and $b_h(t)$ in (3) are associated with the V- and H-pol brightness temperatures, respectively, observed by the radiometer. Their lag cross correlation is given by [12]

$$\langle b_v(t) b_h(t-\tau)\rangle = \left\{ \frac{T_3}{2}\cos(2\pi f_c \tau) - \frac{T_4}{2}\sin(2\pi f_c \tau) \right\} \times \operatorname{sinc}(B\tau). \tag{A1}$$

The time-varying voltages $n_v(t)$ and $n_h(t)$ in (3) are associated with the noise in the V- and H-pol channels of the radiometer

$$\begin{aligned}
\Lambda_{T3.1} &= [\,0 \quad 1 \quad -1 \quad 0\,] \cdot \Lambda_T \cdot [\,0 \quad 1 \quad -1 \quad 0\,]^t \\
&= \frac{G_v^2}{16B\tau} \cdot \left\{ \left[(T_v + T_{Rv})^2 + g^2 (T_h + T_{Rh})^2 \right] (c_p - c_m)^2 + 2\sqrt{g} T_3 \left[(T_v + T_{Rv}) + g(T_h + T_{Rh}) \right] \left(c_p^2 - c_m^2 \right) \right\} \\
&\quad + \frac{G_v^2}{16B\tau} \cdot g \left\{ 2(T_v + T_{Rv})(T_h + T_{Rh})(c_p + c_m)^2 + T_3^2 \left(c_p^2 + c_m^2 \right) - 2T_4^2 c_p c_m \right\} \qquad (19a) \\
\Lambda_{T3.2} &= [\,-1 \quad 2 \quad 0 \quad -1\,] \cdot \Lambda_T \cdot [\,-1 \quad 2 \quad 0 \quad -1\,]^t \\
&= \frac{G_v^2}{8B\tau} \cdot \left\{ 2(T_v + T_{Rv})^2 (c_v - c_p)^2 + 2g^2 (T_h + T_{Rh})^2 (c_h - c_p)^2 + 4g(T_v + T_{Rv})(T_h + T_{Rh}) c_p^2 \right\} \\
&\quad + \frac{G_v^2}{8B\tau} \cdot 4\sqrt{g} T_3 \left[(T_v + T_{Rv}) \left(c_p^2 - c_v c_p \right) + g(T_h + T_{Rh}) \left(c_p^2 - c_h c_p \right) \right] \\
&\quad + \frac{G_v^2}{8B\tau} \cdot g T_3^2 \left(2c_p^2 + c_v c_h - c_v c_p - c_h c_p \right) + g T_4^2 (c_v c_h - c_v c_p - c_h c_p) \qquad (19b) \\
\Lambda_{T3.3} &= [\,1 \quad 0 \quad -2 \quad 1\,] \cdot \Lambda_T \cdot [\,1 \quad 0 \quad -2 \quad 1\,]^t \\
&= \frac{G_v^2}{8B\tau} \cdot \left\{ 2(T_v + T_{Rv})^2 (c_v - c_m)^2 + 2g^2 (T_h + T_{Rh})^2 (c_h - c_m)^2 + 4g(T_v + T_{Rv})(T_h + T_{Rh}) c_m^2 \right\} \\
&\quad + \frac{G_v^2}{8B\tau} \cdot 4\sqrt{g} T_3 \left[(T_v + T_{Rv}) \left(c_v c_m - c_m^2 \right) + g(T_h + T_{Rh}) \left(c_h c_m - c_m^2 \right) \right] \\
&\quad + \frac{G_v^2}{8B\tau} \cdot g T_3^2 \left(2c_m^2 + c_v c_h - c_v c_m - c_h c_m \right) + g T_4^2 \left(c_v c_h - c_v c_m - c_h c_m \right) \qquad (19c)
\end{aligned}$$

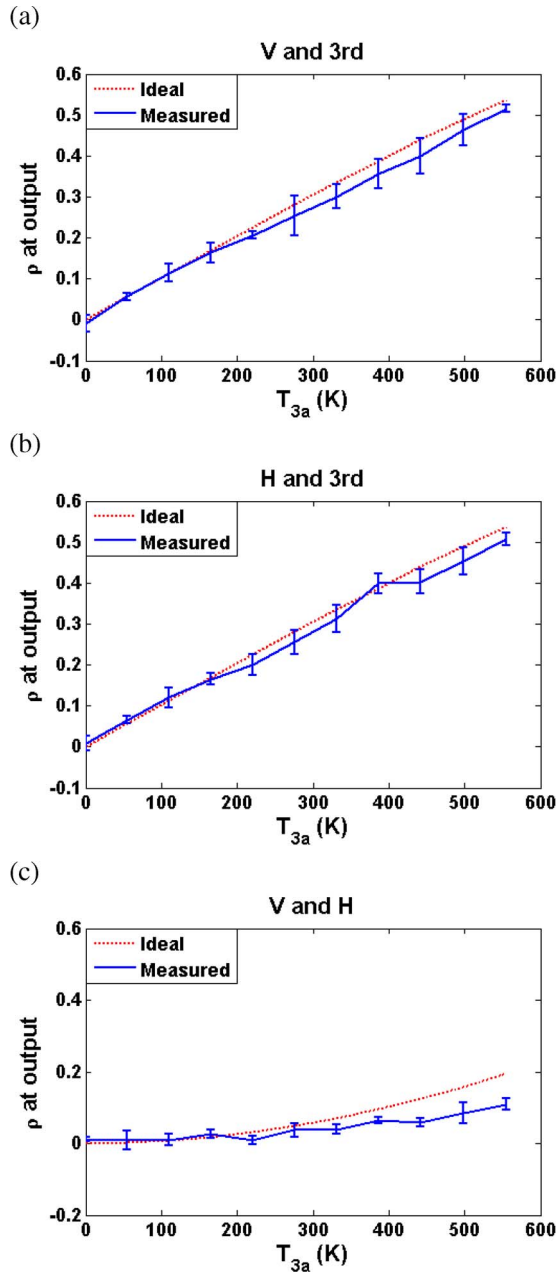

Fig. 3. Correlation between the additive noise in (a) T_v and T_3, (b) T_h and T_3, and (c) T_v and T_h as a function of T_3. $T_4 = 0$ in each case. The theoretical values for the correlation are derived in Sections II and III. The experimental values shown are averages over three independent trials. The error bars represent the standard deviation of the three trials.

hardware. The noise-generating hardware components are, for the most part, distinct between channels, and, therefore, their lag cross correlation also satisfies

$$\langle n_v(t) n_h(t-\tau)\rangle = 0. \tag{A2}$$

The autocorrelation and the lag cross correlation between the signals $v_v(t)$ and $v_h(t)$ in (3) can be expanded as follows:

$$\begin{aligned} R_{v,v}(\tau) &= \langle v_v(t)\cdot v_v(t-\tau)\rangle \\ &= G_v\left\langle [b_v(t)+n_v(t)]\cdot[b_v(t-\tau)+n_v(t-\tau)]\right\rangle \\ &= G_v\left\langle b_v(t)b_v(t-\tau)+n_v(t)n_v(t-\tau)\right\rangle \\ &= G_v\{T_v+T_{Rv}\}\mathrm{sinc}(B\tau)\cos(2\pi f_c\tau) \end{aligned} \tag{A3a}$$

$$\begin{aligned} R_{h,h}(\tau) &= \langle v_h(t)\cdot v_h(t-\tau)\rangle \\ &= G_h\left\langle [b_h(t)+n_h(t)]\cdot[b_h(t-\tau)+n_h(t-\tau)]\right\rangle \\ &= G_h\left\langle b_h(t)b_h(t-\tau)+n_h(t)n_h(t-\tau)\right\rangle \\ &= G_h\{T_h+T_{Rh}\}\mathrm{sinc}(B\tau)\cos(2\pi f_c\tau) \end{aligned} \tag{A3b}$$

$$\begin{aligned} R_{v,h}(\tau) &= \langle v_v(t)\cdot v_h(t-\tau)\rangle \\ &= \sqrt{G_vG_h}\left\langle [b_v(t)+n_v(t)]\cdot[b_h(t-\tau)+n_h(t-\tau)]\right\rangle \\ &= \sqrt{G_vG_h}\left\{\frac{T_3}{2}\cos(2\pi f_c\tau)-\frac{T_4}{2}\sin(2\pi f_c\tau)\right\} \\ &\quad\times\mathrm{sinc}(B\tau) \end{aligned} \tag{A3c}$$

$$\begin{aligned} R_{h,v}(\tau) &= \langle v_h(t)\cdot v_v(t-\tau)\rangle \\ &= \sqrt{G_hG_v}\left\langle [b_h(t)+n_h(t)]\cdot[b_v(t-\tau)+n_v(t-\tau)]\right\rangle \\ &= \sqrt{G_hG_v}\left\{\frac{T_3}{2}\cos(2\pi f_c\tau)+\frac{T_4}{2}\sin(2\pi f_c\tau)\right\} \\ &\quad\times\mathrm{sinc}(B\tau). \end{aligned} \tag{A3d}$$

Useful higher order autocorrelation and cross-correlation statistics for $v_v(t)$ and $v_h(t)$ can be written in terms of the second-order statistics using the identity $\langle abcd\rangle = \langle ab\rangle\langle cd\rangle + \langle ac\rangle\langle bd\rangle + \langle ad\rangle\langle bc\rangle$, which is valid for zero-mean Gaussian-distributed random variables [1]. These higher order moments are given by

$$\begin{aligned} &\left\langle v_v^2(t)v_v^2(t-\tau)\right\rangle \\ &\quad = R_{v,v}^2(0)+2R_{v,v}^2(\tau) \end{aligned} \tag{A4a}$$

$$\begin{aligned} &\left\langle v_v^2(t)v_h^2(t-\tau)\right\rangle \\ &\quad = R_{v,v}(0)R_{h,h}(0)+2R_{v,h}^2(\tau) \end{aligned} \tag{A4b}$$

$$\begin{aligned} &\left\langle v_v^2(t)v_v(t-\tau)v_h(t-\tau)\right\rangle \\ &\quad = R_{v,v}(0)R_{v,h}(0)+2R_{v,v}(\tau)R_{v,h}(\tau) \end{aligned} \tag{A4c}$$

$$\begin{aligned} &\left\langle v_h^2(t)v_h^2(t-\tau)\right\rangle \\ &\quad = R_{h,h}^2(0)+2R_{h,h}^2(\tau) \end{aligned} \tag{A4d}$$

$$\begin{aligned} &\left\langle v_h^2(t)v_v^2(t-\tau)\right\rangle \\ &\quad = R_{v,v}(0)R_{h,h}(0)+2R_{h,v}^2(\tau) \end{aligned} \tag{A4e}$$

$$\begin{aligned} &\left\langle v_{h4}^2(t)v_3(t-\tau)v_4(t-\tau)\right\rangle \\ &\quad = R_{4,4}(0)R_{3,4}(0)+2R_{4,4}(\tau)R_{4,3}(\tau) \end{aligned} \tag{A4f}$$

$$\begin{aligned} &\left\langle v_v(t)v_h(t)v_v^2(t-\tau)\right\rangle \\ &\quad = R_{v,v}(0)R_{v,h}(0)+2R_{v,v}(\tau)R_{h,v}(\tau) \end{aligned} \tag{A4g}$$

$$\begin{aligned} &\left\langle v_v(t)v_h(t)v_h^2(t-\tau)\right\rangle \\ &\quad = R_{h,h}(0)R_{v,h}(0)+2R_{h,h}(\tau)R_{v,h}(\tau) \end{aligned} \tag{A4h}$$

$$\begin{aligned} &\left\langle v_v(t)v_h(t)v_v(t-\tau)v_h(t-\tau)\right\rangle \\ &\quad = R_{v,h}^2(0)+R_{v,v}(\tau)R_{h,h}(\tau)+R_{v,h}(\tau)R_{h,v}(\tau). \end{aligned} \tag{A4i}$$

To derive the autocorrelation and the lag cross correlation of the output signals from the radiometer, i.e., $x_v(t)$, $x_p(t)$, $x_m(t)$, and $x_h(t)$, the autocorrelation and the lag cross correlation of the intermediate signals entering the low-pass filters $w_v(t)$,

$w_p(t)$, $w_m(t)$, and $w_h(t)$ in (10) must first be determined. The autocorrelation of $w_v(t)$ can be expanded as follows:

$$\begin{aligned}R_{wv,wv}(\tau) &= \langle w_v(t)w_v(t-\tau)\rangle \\ &= \frac{c_v^2}{4}\left\langle v_v^2(t)v_v^2(t-\tau)\right\rangle \\ &= \frac{c_v^2}{4}\left\{R_{v,v}^2(0)+2R_{v,v}^2(\tau)\right\} \\ &= \frac{c_v^2G_v^2}{4}(T_v+T_{Rv})^2+\frac{c_v^2G_v^2}{4}(T_v+T_{Rv})^2 \\ &\quad\cdot \operatorname{sinc}^2(B\tau)\left[1+\cos(4\pi f_c\tau)\right] \\ &= \frac{c_v^2G_v^2}{4}(T_v+T_{Rv})^2\left[1+\operatorname{sinc}^2(B\tau)\right] \\ &\quad+\frac{c_v^2G_v^2}{4}(T_v+T_{Rv})^2\operatorname{sinc}^2(B\tau)\cos(4\pi f_c\tau).\end{aligned} \tag{A5a}$$

The cross correlation between $w_v(t)$ and $w_p(t)$ can be expanded as follows:

$$\begin{aligned}R_{wv,wp}(\tau) &= R_{wp,wv}(-\tau)=\langle w_v(t)w_p(t-\tau)\rangle \\ &= \frac{c_vc_p}{8}\left\langle v_v^2(t)\left[v_v(t-\tau)+v_h(t-\tau)\right]^2\right\rangle \\ &= \frac{c_vc_p}{8}\left\langle v_v^2(t)v_v^2(t-\tau)+2v_v^2(t)v_v(t-\tau)\right. \\ &\quad\left.\times v_h(t-\tau)+v_v^2(t)v_h^2(t-\tau)\right\rangle \\ &= \frac{c_vc_p}{8}\left\langle R_{v,v}^2(0)+2R_{v,v}^2(\tau)\right. \\ &\quad+2R_{v,v}(0)R_{v,h}(0)+4R_{v,v}(\tau)R_{v,h}(\tau) \\ &\quad\left.+R_{v,v}(0)R_{h,h}(0)+2R_{v,h}^2(\tau)\right\rangle \\ &= \frac{c_vc_p}{8}G_v^2(T_v+T_{Rv}) \\ &\quad\times\left\{(T_v+T_{Rv})+\sqrt{g}T_3+g(T_h+T_{Rh})\right\} \\ &\quad+\frac{c_vc_p}{8}G_v^2\left\{\left[(T_v+T_{Rv})+\frac{\sqrt{g}}{2}T_3\right]^2+\frac{g}{4}T_4^2\right\} \\ &\quad\times\operatorname{sinc}^2(B\tau) \\ &\quad+\frac{c_vc_p}{8}G_v^2\left\{\left[(T_v+T_{Rv})+\frac{\sqrt{g}}{2}T_3\right]^2-\frac{g}{4}T_4^2\right\} \\ &\quad\times\operatorname{sinc}^2(B\tau)\cos(4\pi f_c\tau) \\ &\quad+\frac{c_vc_p}{8}G_v^2\left\{-\sqrt{g}(T_v+T_{Rv})T_4-\frac{g}{2}T_3T_4\right\} \\ &\quad\times\operatorname{sinc}^2(B\tau)\sin(4\pi f_c\tau).\end{aligned} \tag{A5b}$$

Similarly, the other relevant autocorrelations and lag cross correlations can be expanded as follows:

$$\begin{aligned}&R_{wv,wm}(\tau) \\ &= R_{wm,wv}(-\tau)=\langle V_{wv}(t)V_{wm}(t-\tau)\rangle \\ &= \frac{c_vc_m}{8}\left\langle v_v^2(t)\left[v_v(t-\tau)-v_h(t-\tau)\right]^2\right\rangle \\ &= \frac{c_vc_m}{8}\left\langle v_v^2(t)v_v^2(t-\tau)-2v_v^2(t)v_v(t-\tau)v_h(t-\tau)\right. \\ &\quad\left.+v_v^2(t)v_h^2(t-\tau)\right\rangle \\ &= \frac{c_vc_m}{8}\left\langle R_{v,v}^2(0)+2R_{v,v}^2(\tau)-2R_{v,v}(0)R_{v,h}(0)\right. \\ &\quad\left.-4R_{v,v}(\tau)R_{v,h}(\tau)+R_{v,v}(0)R_{h,h}(0)+2R_{v,h}^2(\tau)\right\rangle \\ &= \frac{c_vc_m}{8}G_v^2(T_v+T_{Rv})\left\{(T_v+T_{Rv})-\sqrt{g}T_3+g(T_h+T_{Rh})\right\} \\ &\quad+\frac{c_vc_m}{8}G_v^2\left\{\left[(T_v+T_{Rv})-\frac{\sqrt{g}}{2}T_3\right]^2+\frac{g}{4}T_4^2\right\}\operatorname{sinc}^2(B\tau) \\ &\quad+\frac{c_vc_m}{8}G_v^2\left\{\left[(T_v+T_{Rv})-\frac{\sqrt{g}}{2}T_3\right]^2-\frac{g}{4}T_4^2\right\} \\ &\quad\times\operatorname{sinc}^2(B\tau)\cos(4\pi f_c\tau) \\ &\quad+\frac{c_vc_m}{8}G_v^2\left\{\sqrt{g}(T_v+T_{Rv})T_4-\frac{g}{2}T_3T_4\right\} \\ &\quad\times\operatorname{sinc}^2(B\tau)\sin(4\pi f_c\tau)\end{aligned} \tag{A5c}$$

$$\begin{aligned}&R_{wv,wh}(\tau) \\ &= R_{wh,wv}(-\tau)=\langle w_v(t)w_h(t-\tau)\rangle \\ &= \frac{c_vc_h}{4}\left\langle v_v^2(t)v_h^2(t-\tau)\right\rangle \\ &= \frac{c_vc_h}{4}\left\{R_{v,v}(0)R_{h,h}(0)+2R_{v,h}^2(\tau)\right\} \\ &= \frac{c_vc_h}{4}G_v^2g(T_v+T_{Rv})(T_h+T_{Rh}) \\ &\quad+\frac{c_vc_h}{16}G_v^2g\left\{T_3^2+T_4^2\right\}\operatorname{sinc}^2(B\tau) \\ &\quad+\frac{c_vc_h}{16}G_v^2g\left\{T_3^2-T_4^2\right\}\operatorname{sinc}^2(B\tau)\cos(4\pi f_c\tau) \\ &\quad+\frac{c_vc_h}{16}G_v^2g\{-2T_3T_4\}\operatorname{sinc}^2(B\tau)\sin(4\pi f_c\tau)\end{aligned} \tag{A5d}$$

$$\begin{aligned}&R_{wp,wp}(\tau) \\ &= \langle w_p(t)w_p(t-\tau)\rangle \\ &= \frac{c_p^2}{16}\left\langle\left[v_v(t)+v_h(t)\right]^2\left[v_v(t-\tau)+v_h(t-\tau)\right]^2\right\rangle \\ &= \frac{c_p^2}{16}\left\langle\left[v_v^2(t)+v_h^2(t)+2v_v(t)\cdot v_h(t)\right]\right. \\ &\quad\left.\cdot\left[v_v^2(t-\tau)+v_h^2(t-\tau)+2v_v(t-\tau)\cdot v_h(t-\tau)\right]\right\rangle \\ &= \frac{c_p^2}{16}\left\{R_{v,v}^2(0)+2R_{v,v}(0)R_{h,h}(0)+R_{h,h}^2(0)\right. \\ &\quad\left.+4R_{v,v}(0)R_{v,h}(0)+4R_{h,h}(0)R_{v,h}(0)+4R_{v,h}^2(0)\right\} \\ &\quad+\frac{c_p^2}{16}\left\{2R_{v,v}^2(\tau)+2R_{v,h}^2(\tau)+2R_{h,v}^2(\tau)+2R_{h,h}^2(\tau)\right\} \\ &\quad+\frac{c_p^2}{16}\left\{4R_{v,v}(\tau)R_{v,h}(\tau)+4R_{v,v}(\tau)R_{h,v}(\tau)\right. \\ &\quad\left.+4R_{v,v}(\tau)R_{h,h}(\tau)\right\} \\ &\quad+\frac{c_p^2}{16}\left\{4R_{h,h}(\tau)R_{v,h}(\tau)+4R_{h,h}(\tau)R_{h,v}(\tau)\right. \\ &\quad\left.+4R_{v,h}(\tau)R_{h,v}(\tau)\right\}\end{aligned}$$

$$
\begin{aligned}
&= \frac{c_p^2}{16} G_v^2 \left\{ (T_v + T_{Rv}) + g(T_h + T_{Rh}) + \sqrt{g} T_3 \right\}^2 \\
&\quad + \frac{c_p^2}{16} G_v^2 \left\{ (T_v + T_{Rv}) + g(T_h + T_{Rh}) + \sqrt{g} T_3 \right\}^2 \operatorname{sinc}^2(B\tau) \\
&\quad + \frac{c_p^2}{16} G_v^2 \left\{ (T_v + T_{Rv}) + g(T_h + T_{Rh}) + \sqrt{g} T_3 \right\}^2 \\
&\qquad \times \operatorname{sinc}^2(B\tau) \cos(4\pi f_c \tau) \qquad \text{(A5e)}
\end{aligned}
$$

$$
\begin{aligned}
&R_{wp,wm}(\tau) \\
&= R_{wm,wp}(-\tau) = \langle w_p(t) w_m(t-\tau) \rangle \\
&= \frac{c_p c_m}{16} \left\langle \left[v_v(t) + v_h(t) \right]^2 \left[v_v(t-\tau) - v_h(t-\tau) \right]^2 \right\rangle \\
&= \frac{c_p c_m}{16} \left\langle \left[v_v^2(t) + v_h^2(t) + 2 v_v(t) \cdot v_h(t) \right] \right. \\
&\qquad \left. \cdot \left[v_v^2(t-\tau) + v_h^2(t-\tau) - 2 v_v(t-\tau) \cdot v_h(t-\tau) \right] \right\rangle \\
&= \frac{c_p c_m}{16} \left\{ R_{v,v}^2(0) + 2 R_{v,v}(0) R_{h,h}(0) + R_{h,h}^2(0) - 4 R_{v,h}^2(0) \right\} \\
&\quad + \frac{c_p c_m}{16} \left\{ 2 R_{v,v}^2(\tau) + 2 R_{v,h}^2(\tau) + 2 R_{h,v}^2(\tau) + 2 R_{h,h}^2(\tau) \right\} \\
&\quad + \frac{c_p c_m}{16} \left\{ -4 R_{v,v}(\tau) R_{v,h}(\tau) + 4 R_{v,v}(\tau) R_{h,v}(\tau) \right. \\
&\qquad \left. - 4 R_{v,v}(\tau) R_{h,h}(\tau) \right\} \\
&\quad + \frac{c_p c_m}{16} \left\{ -4 R_{h,h}(\tau) R_{h,v}(\tau) + 4 R_{h,h}(\tau) R_{v,h}(\tau) \right. \\
&\qquad \left. - 4 R_{v,h}(\tau) R_{h,v}(\tau) \right\} \\
&= \frac{c_p c_m}{16} G_v^2 \left\{ \left[(T_v + T_{Rv}) + g(T_h + T_{Rh}) \right]^2 - g T_3^2 \right\} \\
&\quad + \frac{c_p c_m}{16} G_v^2 \left\{ \left[(T_v + T_{Rv}) - g(T_h + T_{Rh}) \right]^2 + g T_4^2 \right\} \times \operatorname{sinc}^2(B\tau) \\
&\quad + \frac{c_p c_m}{16} G_v^2 \left\{ \left[(T_v + T_{Rv}) - g(T_h + T_{Rh}) \right]^2 - g T_4^2 \right\} \\
&\qquad \times \operatorname{sinc}^2(B\tau) \cos(4\pi f_c \tau) \\
&\quad + \frac{c_p c_m}{8} G_v^2 \sqrt{g} \left\{ (T_v + T_{Rv}) - g(T_h + T_{Rh}) \right\} T_4 \\
&\qquad \times \operatorname{sinc}^2(B\tau) \sin(4\pi f_c \tau) \qquad \text{(A5f)}
\end{aligned}
$$

$$
\begin{aligned}
&R_{wp,wh}(\tau) \\
&= R_{wh,wp}(-\tau) \\
&= \langle w_p(t) w_h(t-\tau) \rangle = \frac{c_p c_h}{8} \left\langle \left[v_v(t) + v_h(t) \right]^2 v_h^2(t-\tau) \right\rangle \\
&= \frac{c_p c_h}{8} \left\langle v_v^2(t) v_h^2(t-\tau) + v_h^2(t) v_h^2(t-\tau) + 2 v_v(t) \cdot v_h(t) v_h^2(t-\tau) \right\rangle \\
&= \frac{c_p c_h}{8} \left\{ 2 R_{v,v}(0) R_{h,h}(0) + 4 R_{v,h}^2(\tau) + 2 R_{h,h}^2(0) + 4 R_{h,h}^2(\tau) \right. \\
&\qquad \left. + 4 R_{h,h}(0) R_{v,h}(0) + 8 R_{h,h}(\tau) R_{v,h}(\tau) \right\} \\
&= \frac{c_p c_h}{8} G_v^2 g (T_h + T_{Rh}) \left\{ (T_v + T_{Rv}) + g(T_h + T_{Rh}) + \sqrt{g} T_3 \right\} \\
&\quad + \frac{c_p c_h}{8} G_v^2 \left\{ \left[g(T_h + T_{Rh}) + \frac{\sqrt{g}}{2} T_3 \right]^2 + \frac{g}{4} T_4^2 \right\} \operatorname{sinc}^2(B\tau) \\
&\quad + \frac{c_p c_h}{8} G_v^2 \left\{ \left[g(T_h + T_{Rh}) + \frac{\sqrt{g}}{2} T_3 \right]^2 - \frac{g}{4} T_4^2 \right\} \\
&\qquad \times \operatorname{sinc}^2(B\tau) \cos(4\pi f_c \tau) \\
&\quad + \frac{c_p c_h}{8} G_v^2 g \left\{ -\frac{T_3}{2} - \sqrt{g}(T_h + T_{Rh}) \right\} \\
&\qquad \times T_4 \operatorname{sinc}^2(B\tau) \sin(4\pi f_c \tau) \qquad \text{(A5g)}
\end{aligned}
$$

$$
\begin{aligned}
&R_{wm,wm}(\tau) \\
&= \langle w_m(t) w_m(t-\tau) \rangle \\
&= \frac{c_m^2}{16} \left\langle \left[v_v(t) - v_h(t) \right]^2 \left[v_v(t-\tau) - v_h(t-\tau) \right]^2 \right\rangle \\
&= \frac{c_m^2}{16} \left\langle \left[v_v^2(t) + v_h^2(t) - 2 v_v(t) \cdot v_h(t) \right] \right. \\
&\qquad \left. \cdot \left[v_v^2(t-\tau) + v_v^2(t-\tau) - 2 v_v(t-\tau) \cdot v_h(t-\tau) \right] \right\rangle \\
&= \frac{c_m^2}{16} \left\{ R_{v,v}^2(0) + 2 R_{v,v}(0) R_{h,h}(0) + R_{h,h}^2(0) \right. \\
&\qquad \left. - 4 R_{v,v}(0) R_{v,h}(0) - 4 R_{h,h}(0) R_{v,h}(0) + 4 R_{v,h}^2(0) \right\} \\
&\quad + \frac{c_m^2}{16} \left\{ 2 R_{v,v}^2(\tau) + 2 R_{v,h}^2(\tau) + 2 R_{h,v}^2(\tau) + 2 R_{h,h}^2(\tau) \right\} \\
&\quad + \frac{c_m^2}{16} \left\{ -4 R_{v,v}(\tau) R_{v,h}(\tau) - 4 R_{v,v}(\tau) R_{h,v}(\tau) \right. \\
&\qquad \left. + 4 R_{v,v}(\tau) R_{h,h}(\tau) \right\} \\
&\quad + \frac{c_m^2}{16} \left\{ -4 R_{h,h}(\tau) R_{v,h}(\tau) \right. \\
&\qquad \left. - 4 R_{h,h}(\tau) R_{h,v}(\tau) + 4 R_{v,h}(\tau) R_{h,v}(\tau) \right\} \\
&= \frac{c_m^2}{16} G_v^2 \left\{ (T_v + T_{Rv}) + g(T_h + T_{Rh}) - \sqrt{g} T_3 \right\}^2 \\
&\quad + \frac{c_m^2}{16} G_v^2 \left\{ (T_v + T_{Rv}) + g(T_h + T_{Rh}) - \sqrt{g} T_3 \right\}^2 \operatorname{sinc}^2(B\tau) \\
&\quad + \frac{c_m^2}{16} G_v^2 \left\{ (T_v + T_{Rv}) + g(T_h + T_{Rh}) - \sqrt{g} T_3 \right\}^2 \\
&\qquad \times \operatorname{sinc}^2(B\tau) \cos(4\pi f_c \tau) \qquad \text{(A5h)}
\end{aligned}
$$

$$
\begin{aligned}
&R_{wm,wh}(\tau) \\
&= R_{wh,wm}(-\tau) = \langle w_m(t) w_h(t-\tau) \rangle \\
&= \frac{c_m c_h}{8} \left\langle \left[v_v(t) - v_h(t) \right]^2 v_h^2(t-\tau) \right\rangle \\
&= \frac{c_m c_h}{8} \left\langle v_v^2(t) v_h^2(t-\tau) + v_h^2(t) v_h^2(t-\tau) - 2 v_v(t) \right. \\
&\qquad \left. \cdot v_h(t) v_h^2(t-\tau) \right\rangle \\
&= \frac{c_m c_h}{8} \left\{ R_{v,v}(0) R_{h,h}(0) + 2 R_{v,h}^2(\tau) + R_{h,h}^2(0) + 2 R_{h,h}^2(\tau) \right. \\
&\qquad \left. - 2 R_{h,h}(0) R_{v,h}(0) - 4 R_{h,h}(\tau) R_{v,h}(\tau) \right\} \\
&= \frac{c_m c_h}{8} G_v^2 g (T_h + T_{Rv}) \left\{ (T_v + T_{Rv}) + g(T_h + T_{Rh}) - \sqrt{g} T_3 \right\} \\
&\quad + \frac{c_m c_h}{8} G_v^2 \left\{ \left[g(T_h + T_{Rh}) - \frac{\sqrt{g}}{2} T_3 \right]^2 + \frac{g}{4} T_4^2 \right\} \operatorname{sinc}^2(B\tau) \\
&\quad + \frac{c_m c_h}{8} G_v^2 \left\{ \left[g(T_h + T_{Rh}) - \frac{\sqrt{g}}{2} T_3 \right]^2 - \frac{g}{4} T_4^2 \right\} \\
&\qquad \times \operatorname{sinc}^2(B\tau) \cos(4\pi f_c \tau) \\
&\quad + \frac{c_m c_h}{8} G_v^2 g \left\{ -\frac{T_3}{2} + \sqrt{g}(T_h + T_{Rh}) \right\} \\
&\qquad \times T_4 \operatorname{sinc}^2(B\tau) \sin(4\pi f_c \tau) \qquad \text{(A5i)}
\end{aligned}
$$

$$
\begin{aligned}
&R_{wh,wh}(\tau) \\
&= \langle w_h(t) w_h(t-\tau) \rangle = \frac{c_h^2}{4} \left\langle v_h^2(t) v_h^2(t-\tau) \right\rangle \\
&= \frac{c_h^2}{4} \left\{ R_{h,h}^2(0) + 2 R_{h,h}^2(\tau) \right\} \\
&= \frac{c_h^2}{4} G_v^2 g^2 (T_h + T_{Rh})^2 \left[1 + \operatorname{sinc}^2(B\tau) \right] \\
&\quad + \frac{c_h^2}{4} G_v^2 g^2 (T_h + T_{Rh})^2 \operatorname{sinc}^2(B\tau) \cos(4\pi f_c \tau). \qquad \text{(A5j)}
\end{aligned}
$$

Spectra and Cross Spectra

The power spectra and the cross spectra of the radiometer signals are found as Fourier transforms of their autocorrelations and lag cross correlations. For signals $w_v(t)$, $w_p(t)$, $w_m(t)$, and $w_h(t)$, the power spectra and the cross spectra are given by

$$S_{wv,wv}(f) = \frac{c_v^2}{4}G_v^2(T_v+T_{Rv})^2\delta(f)+\frac{c_v^2}{4}G_v^2(T_v+T_{Rv})^2H(f) \tag{A6a}$$

$$\begin{aligned}S_{wv,wp}(f) &= \frac{c_vc_p}{8}G_v^2(T_v+T_{Rv})\{(T_v+T_{Rv})+g(T_h+T_{Rh})+\sqrt{g}T_3\}\delta(f)\\ &\quad+\frac{c_vc_p}{8}G_v^2\left\{\left[(T_v+T_{Rv})+\frac{\sqrt{g}}{2}T_3\right]^2+\frac{g}{4}T_4^2\right\}H(f)\end{aligned} \tag{A6b}$$

$$\begin{aligned}S_{wv,wm}(f) &= \frac{c_vc_m}{8}G_v^2(T_v+T_{Rv})\\ &\quad\times\{(T_v+T_{Rv})+g(T_h+T_{Rh})-\sqrt{g}T_3\}\,\delta(f)\\ &\quad+\frac{c_vc_m}{8}G_v^2\left\{\left[(T_v+T_{Rv})-\frac{\sqrt{g}}{2}T_3\right]^2+\frac{g}{4}T_4^2\right\}H(f)\end{aligned} \tag{A6c}$$

$$\begin{aligned}S_{wv,wh}(f) &= \frac{c_vc_h}{4}G_v^2g(T_v+T_{Rv})(T_h+T_{Rh})\delta(f)\\ &\quad+\frac{c_vc_h}{16}G_v^2g\left\{T_3^2+T_4^2\right\}H(f)\end{aligned} \tag{A6d}$$

$$\begin{aligned}S_{wp,wp}(f) &= \frac{c_p^2}{16}G_v^2\left\{(T_v+T_{Rv})+g(T_h+T_{Rh})+\sqrt{g}T_3\right\}^2\delta(f)\\ &\quad+\frac{c_p^2}{16}G_v^2\left\{(T_v+T_{Rv})+g(T_h+T_{Rh})+\sqrt{g}T_3\right\}^2H(f)\end{aligned} \tag{A6e}$$

$$\begin{aligned}S_{wp,wm}(f) &= \frac{c_pc_m}{16}G_v^2\left\{[(T_v+T_{Rv})+g(T_h+T_{Rh})]^2-gT_3^2\right\}\delta(f)\\ &\quad+\frac{c_pc_m}{16}G_v^2\left\{[(T_v+T_{Rv})-g(T_h+T_{Rh})]^2+gT_4^2\right\}H(f)\end{aligned} \tag{A6f}$$

$$\begin{aligned}S_{wp,wh}(f) &= \frac{c_pc_h}{8}G_v^2g(T_h+T_{Rh})\\ &\quad\times\{(T_v+T_{Rv})+g(T_h+T_{Rh})+\sqrt{g}T_3\}\,\delta(f)\\ &\quad+\frac{c_pc_h}{8}G_v^2\left\{\left[g(T_h+T_{Rh})+\frac{\sqrt{g}}{2}T_3\right]^2+\frac{g}{4}T_4^2\right\}H(f)\end{aligned} \tag{A6g}$$

$$\begin{aligned}S_{wm,wm}(f) &= \frac{c_m^2}{16}G_v^2\left\{(T_v+T_{Rv})+g(T_h+T_{Rh})-\sqrt{g}T_3\right\}^2\delta(f)\\ &\quad+\frac{c_m^2}{16}G_v^2\left\{(T_v+T_{Rv})+g(T_h+T_{Rh})-\sqrt{g}T_3\right\}^2H(f)\end{aligned} \tag{A6h}$$

$$\begin{aligned}S_{wm,wh}(f) &= \frac{c_mc_h}{8}G_v^2g(T_h+T_{Rh})\\ &\quad\times\{(T_v+T_{Rv})+g(T_h+T_{Rh})-\sqrt{g}T_3\}\,\delta(f)\\ &\quad+\frac{c_mc_h}{8}G_v^2\left\{\left[g(T_h+T_{Rh})-\frac{\sqrt{g}}{2}T_3\right]^2+\frac{g}{4}T_4^2\right\}H(f)\end{aligned} \tag{A6i}$$

$$S_{wh,wh}(f) = \frac{c_h^2}{4}G_v^2g^2(T_h+T_{Rh})^2\delta(f)+\frac{c_h^2}{4}G_v^2g^2(T_h+T_{Rh})^2H(f) \tag{A6j}$$

where the Fourier transforms of the terms modulated by $\cos(4\pi f_c\tau)$ in the expressions for the autocorrelation and the lag cross correlation given in (A5a)–(A5j) are not included here because they will be removed by the subsequent low-pass filters. In (A6a)–(A6j), $g = G_h/G_v$ is the gain imbalance between V- and H-pol channels, $S_{wa,wa}(f)$ is the spectrum of $w_a(t)$, and $S_{wa,wb}(f)$ is the cross spectrum of $w_a(t)$ and $w_b(t)$. The "hat" function $H(f)$ in (A6a)–(A6j) is given by

$$\begin{cases}H(f) = \frac{1}{B}\left(1-\left|\frac{f}{B}\right|\right) & \text{for } |f|\langle B\\ = 0 & \text{otherwise.}\end{cases} \tag{A7}$$

The power spectra and the cross spectra of signals $x_v(t)$, $x_p(t)$, $x_m(t)$, and $x_h(t)$ at the output of the low-pass filters can be found from (A6) by

$$S_{a,b}(f) = S_{wa,wb}(f)\cdot|L(f)|^2 \tag{A8}$$

where $a = v$, h, p, and m, and $L(f)$ is the transfer function of the low-pass filter, defined as zero for $|f| \geq 1/2\tau$ and one otherwise, where τ is the integration time. Near dc, the hat function $H(f)$ can be approximated by its value at $f = 0$. The power spectra at $|f| < 1/2\tau$ are given by

$$S_{v,v}(f) = \frac{c_v^2}{4}G_v^2(T_v+T_{Rv})^2\delta(f)+\frac{c_v^2}{4B}G_v^2\,(T_v+T_{Rv})^2 \tag{A9a}$$

$$\begin{aligned}S_{v,p}(f) &= \frac{c_vc_p}{8}G_v^2(T_v+T_{Rv})\\ &\quad\times\{(T_v+T_{Rv})+g(T_h+T_{Rh})+\sqrt{g}T_3\}\,\delta(f)\\ &\quad+\frac{c_vc_p}{8B}G_v^2\left\{\left[(T_v+T_{Rv})+\frac{\sqrt{g}}{2}T_3\right]^2+\frac{g}{4}T_4^2\right\}\end{aligned} \tag{A9b}$$

$$S_{v,m}(f) = \frac{c_v c_m}{8} G_v^2 (T_v + T_{Rv}) \times \{(T_v + T_{Rv}) + g(T_h + T_{Rh}) - \sqrt{g} T_3\} \delta(f) + \frac{c_v c_m}{8B} G_v^2 \left\{ \left[(T_v + T_{Rv}) - \frac{\sqrt{g}}{2} T_3 \right]^2 + \frac{g}{4} T_4^2 \right\} \quad \text{(A9c)}$$

$$S_{v,h}(f) = \frac{c_v c_h}{4} G_v^2 g (T_v + T_{Rv})(T_h + T_{Rh}) \delta(f) + \frac{c_v c_h}{16B} G_v^2 g \left\{ T_3^2 + T_4^2 \right\} \quad \text{(A9d)}$$

$$S_{p,p}(f) = \frac{c_p^2}{16} G_v^2 \left\{ (T_v + T_{Rv}) + g(T_h + T_{Rh}) + \sqrt{g} T_3 \right\}^2 \delta(f) + \frac{c_p^2}{16B} G_v^2 \left\{ (T_v + T_{Rv}) + g(T_h + T_{Rh}) + \sqrt{g} T_3 \right\}^2 \quad \text{(A9e)}$$

$$S_{p,m}(f) = \frac{c_p c_m}{16} G_v^2 \Big\{ \left[(T_v + T_{Rv}) + g(T_h + T_{Rh}) \right]^2 - g T_3^2 \Big\} \delta(f) + \frac{c_p c_m}{16B} G_v^2 \left\{ \left[(T_v + T_{Rv}) - g(T_h + T_{Rh}) \right]^2 + g T_4^2 \right\} \quad \text{(A9f)}$$

$$S_{p,h}(f) = \frac{c_p c_h}{8} G_v^2 g (T_h + T_{Rh}) \times \{(T_v + T_{Rv}) + g(T_h + T_{Rh}) + \sqrt{g} T_3\} \delta(f) + \frac{c_p c_h}{8B} G_v^2 \left\{ \left[g(T_h + T_{Rh}) + \frac{\sqrt{g}}{2} T_3 \right]^2 + \frac{g}{4} T_4^2 \right\} \quad \text{(A9g)}$$

$$S_{m,m}(f) = \frac{c_m^2}{16} G_v^2 \left\{ (T_v + T_{Rv}) + g(T_h + T_{Rh}) - \sqrt{g} T_3 \right\}^2 \delta(f) + \frac{c_m^2}{16B} G_v^2 \left\{ (T_v + T_{Rv}) + g(T_h + T_{Rh}) - \sqrt{g} T_3 \right\}^2 \quad \text{(A9h)}$$

$$S_{m,h}(f) = v \frac{c_m c_h}{8} G_v^2 g (T_h + T_{Rh}) \times \{(T_v + T_{Rv}) + g(T_h + T_{Rh}) - \sqrt{g} T_3\} \delta(f) + \frac{c_m c_h}{8B} G_v^2 \left\{ \left[g(T_h + T_{Rh}) - \frac{\sqrt{g}}{2} T_3 \right]^2 + \frac{g}{4} T_4^2 \right\} \quad \text{(A9i)}$$

$$S_{h,h}(f) = \frac{c_h^2}{4} G_v^2 g^2 (T_h + T_{Rh})^2 \delta(f) + \frac{c_h^2}{4B} G_v^2 g^2 (T_h + T_{Rh})^2. \quad \text{(A9j)}$$

In the above expressions, the terms on the right-hand side that involve the Dirac delta function $\delta(f)$ are the dc components of the spectrum. The other terms are the ac components.

The power contained in the dc and ac frequency components of $x_v(t)$, $x_p(t)$, $x_m(t)$, and $x_h(t)$ are obtained by integrating over the appropriate portions of their spectra. The expected values of these signals (i.e., the dc component of their spectra) are proportional to the four associated brightness temperatures. The variance of the signals (i.e., the integral over all ac components of the spectra) is due to the additive noise present in the measurements. The expected value (dc) and variance (ac) are separately given as follows:

$$R_{v,v}^{\mathrm{dc}}(0) = \frac{c_v^2}{4} G_v^2 (T_v + T_{Rv})^2$$
$$R_{v,v}^{\mathrm{ac}}(0) = \frac{c_v^2}{4B\tau} G_v^2 (T_v + T_{Rv})^2 \quad \text{(A10a)}$$

$$R_{v,p}^{\mathrm{dc}}(0) = \frac{c_v c_p}{8} G_v^2 (T_v + T_{Rv}) \times \{(T_v + T_{Rv}) + g(T_h + T_{Rv}) + \sqrt{g} T_3\}$$
$$R_{v,p}^{\mathrm{ac}}(0) = \frac{c_v c_p}{8B\tau} G_v^2 \left\{ \left[(T_v + T_{Rv}) + \frac{\sqrt{g}}{2} T_3 \right]^2 + \frac{g}{4} T_4^2 \right\} \quad \text{(A10b)}$$

$$R_{v,m}^{\mathrm{dc}}(0) = \frac{c_v c_m}{8} G_v^2 (T_v + T_{Rv}) \times \{(T_v + T_{Rv}) + g(T_h + T_{Rh}) - \sqrt{g} T_3\}$$
$$R_{v,m}^{\mathrm{ac}}(0) = \frac{c_v c_m}{8B\tau} G_v^2 \left\{ \left[(T_v + T_{Rv}) - \frac{\sqrt{g}}{2} T_3 \right]^2 + \frac{g}{4} T_4^2 \right\} \quad \text{(A10c)}$$

$$R_{v,h}^{\mathrm{dc}}(0) = \frac{c_v c_h}{4} G_v^2 g (T_v + T_{Rv})(T_h + T_{Rh})$$
$$R_{v,h}^{\mathrm{ac}}(0) = \frac{c_v c_h}{16B\tau} G_v^2 g \left\{ T_3^2 + T_4^2 \right\} \quad \text{(A10d)}$$

$$R_{p,p}^{\mathrm{dc}}(0) = \frac{c_p^2}{16} G_v^2 \left\{ (T_v + T_{Rv}) + g(T_h + T_{Rh}) + \sqrt{g} T_3 \right\}^2$$
$$R_{p,p}^{\mathrm{ac}}(0) = \frac{c_p^2}{16B\tau} G_v^2 \left\{ (T_v + T_{Rv}) + g(T_h + T_{Rh}) + \sqrt{g} T_3 \right\}^2 \quad \text{(A10e)}$$

$$R_{p,m}^{\mathrm{dc}}(0) = \frac{c_p c_m}{16} G_v^2 \left\{ \left[(T_v + T_{Rv}) + g(T_h + T_{Rh}) \right]^2 - g T_3^2 \right\}$$
$$R_{p,m}^{\mathrm{ac}}(0) = \frac{c_p c_m}{16B\tau} G_v^2 \left\{ \left[(T_v + T_{Rv}) - g(T_h + T_{Rh}) \right]^2 + g T_4^2 \right\} \quad \text{(A10f)}$$

$$R_{p,h}^{\mathrm{dc}}(0) = \frac{c_p c_h}{8} G_v^2 g (T_h + T_{Rh}) \times \{(T_v + T_{Rv}) + g(T_h + T_{Rh}) + \sqrt{g} T_3\}$$
$$R_{p,h}^{\mathrm{ac}}(0) = \frac{c_p c_h}{8B\tau} G_v^2 \left\{ \left[g(T_h + T_{Rh}) + \frac{\sqrt{g}}{2} T_3 \right]^2 + \frac{g}{4} T_4^2 \right\} \quad \text{(A10g)}$$

$$R^{\rm dc}_{m,m}(0)=\frac{c_m^2}{16}G_v^2\left\{(T_v+T_{Rv})+g(T_h+T_{Rh})-\sqrt{g}T_3\right\}^2$$

$$R^{\rm ac}_{m,m}(0)=\frac{c_m^2}{16B\tau}G_v^2\left\{(T_v+T_{Rv})+g(T_h+T_{Rh})-\sqrt{g}T_3\right\}^2 \tag{A10h}$$

$$R^{\rm dc}_{m,h}(0)=\frac{c_m c_h}{8}G_v^2 g(T_h+T_{Rh}) \times\left\{(T_v+T_{Rv})+g(T_h+T_{Rh})-\sqrt{g}T_3\right\}$$

$$R^{\rm ac}_{m,h}(0)=\frac{c_m c_h}{8B\tau}G_v^2\left\{\left[g(T_h+T_{Rh})-\frac{\sqrt{g}}{2}T_3\right]^2+\frac{g}{4}T_4^2\right\} \tag{A10i}$$

$$R^{\rm dc}_{h,h}(0)=\frac{c_h^2}{4}G_v^2 g^2(T_h+T_{Rh})^2$$

$$R^{\rm ac}_{h,h}(0)=\frac{c_h^2}{4B\tau}G_v^2 g^2(T_h+T_{Rh})^2. \tag{A10j}$$

APPENDIX B
COVARIANCE OF CORRELATING POLARIMETRIC RADIOMETER SIGNALS

The signals $v_v(t)-v_6(t)$, $n_v(t)$, $n_h(t)$, $b_v(t)$, and $b_h(t)$ and their statistical properties are identical to those associated with Appendix A. The signal in the cross-correlating channel of the radiometer, prior to low-pass filtering, is given by

$$w_3(t)=v_v(t)\cdot v_h(t). \tag{B1}$$

After the low-pass filter, the correlating channel signal becomes $x_3(t)$.

The procedure that is followed to derive the covariance relationships between the three low-pass-filtered signals is similar to that for the hybrid-combining radiometer, as described in Appendix A. The autocorrelations and the lag cross correlations between signals $w_v(t)$, $w_h(t)$, and $w_3(t)$ can be expanded as follows:

$$\begin{aligned}R_{wv,wv}(\tau)&=\langle w_v(t)w_v(t-\tau)\rangle\\&=\left\langle v_v^2(t)v_v^2(t-\tau)\right\rangle\\&=R_{v,v}^2(0)+2R_{v,v}^2(\tau)\\&=G_v^2(T_v+T_{Rv})^2+G_v^2(T_v+T_{Rv})^2\\&\quad\times\operatorname{sinc}^2(B\tau)\left\{1+\cos(4\pi f_c\tau)\right\}\end{aligned} \tag{B2a}$$

$$\begin{aligned}R_{wv,w3}(\tau)&=R_{w3,wv}(-\tau)=\langle w_v(t)w_3(t-\tau)\rangle\\&=\left\langle v_v^2(t)v_v(t-\tau)\cdot v_h(t-\tau)\right\rangle\\&=R_{v,v}(0)R_{v,h}(0)+2R_{v,v}(\tau)R_{v,h}(\tau)\\&=\frac{\sqrt{g}}{2}G_v^2(T_v+T_{Rv})T_3\\&\quad+\frac{\sqrt{g}}{2}G_v^2(T_v+T_{Rv})\operatorname{sinc}^2(B\tau)T_3\\&\quad+\frac{\sqrt{g}}{2}G_v^2(T_v+T_{Rv})\\&\quad\times\operatorname{sinc}^2(B\tau)\left\{T_3\cos(4\pi f_c\tau)-T_4\sin(4\pi f_c\tau)\right\}\end{aligned} \tag{B2b}$$

$$\begin{aligned}R_{wv,wh}(\tau)&=R_{wh,wv}(-\tau)=\langle w_v(t)w_h(t-\tau)\rangle\\&=\left\langle v_v^2(t)v_h^2(t-\tau)\right\rangle\\&=R_{v,v}(0)R_{h,h}(0)+2R_{v,h}^2(\tau)\\&=gG_v^2(T_v+T_{Rv})(T_h+T_{Rh})\\&\quad+\frac{g}{4}G_v^2\operatorname{sinc}^2(B\tau)\left\{T_3^2+T_4^2\right\}+\frac{g}{4}G_v^2\operatorname{sinc}^2(B\tau)\\&\quad\times\left\{(T_3^2-T_4^2)\cos(4\pi f_c\tau)-2T_3T_4\sin(4\pi f_c\tau)\right\}\end{aligned} \tag{B2c}$$

$$\begin{aligned}R_{w3,w3}(\tau)&=\langle w_3(t)w_3(t-\tau)\rangle\\&=\langle v_v(t)\cdot v_h(t)v_v(t-\tau)\cdot v_h(t-\tau)\rangle\\&=R_{v,h}^2(0)+R_{v,v}(\tau)R_{h,h}(\tau)+R_{v,h}(\tau)R_{h,v}(\tau)\\&=\frac{g}{4}G_v^2T_3^2+0.5gG_v^2(T_v+T_{Rv})(T_h+T_{Rh})\\&\quad\times\operatorname{sinc}^2(B\tau)\left\{1+\cos(4\pi f_c\tau)\right\}+\frac{g}{8}G_v^2\operatorname{sinc}^2(B\tau)\\&\quad\times\left\{T_3^2-T_4^2+(T_3^2+T_4^2)\cos(4\pi f_c\tau)\right\}\end{aligned} \tag{B2d}$$

$$\begin{aligned}R_{w3,wh}(\tau)&=R_{wh,w3}(-\tau)=\langle w_3(t)w_h(t-\tau)\rangle\\&=\left\langle v_v(t)\cdot v_h(t)v_h^2(t-\tau)\right\rangle\\&=R_{v,h}(0)R_{h,h}(0)+2R_{v,h}(\tau)R_{h,h}(\tau)\\&=\frac{\sqrt{g^3}}{2}G_v^2(T_h+T_{Rh})T_3\\&\quad+\frac{\sqrt{g^3}}{2}G_v^2(T_h+T_{Rh})\operatorname{sinc}^2(B\tau)\\&\quad\times\left\{T_3+T_3\cos(4\pi f_c\tau)-T_4\sin(4\pi f_c\tau)\right\}\end{aligned} \tag{B2e}$$

$$\begin{aligned}R_{wh,wh}(\tau)&=\langle w_h(t)w_h(t-\tau)\rangle=\left\langle v_h^2(t)v_h^2(t-\tau)\right\rangle\\&=R_{h,h}^2(0)+2R_{h,h}^2(\tau)\\&=g^2G_v^2(T_h+T_{Rh})^2+g^2G_v^2(T_h+T_{Rh})^2\\&\quad\times\operatorname{sinc}^2(B\tau)\left\{1+\cos(4\pi f_c\tau)\right\}.\end{aligned} \tag{B2f}$$

The power spectra and the cross spectra of the radiometer signals are the Fourier transforms of their autocorrelations and lag cross correlations, respectively. For signals $w_v(t)$, $w_h(t)$, and $w_3(t)$, the power spectra and the cross spectra are given by

$$S_{wv,wv}(f)=G_v^2(T_v+T_{Rv})^2\delta(f)+G_v^2(T_v+T_{Rv})^2H(f) \tag{B3a}$$

$$S_{wv,w3}(f)=\frac{\sqrt{g}}{2}G_v^2(T_v+T_{Rv})T_3\delta(f)+\frac{\sqrt{g}}{2}G_v^2(T_v+T_{Rv})T_3H(f) \tag{B3b}$$

$$S_{wv,wh}(f)=gG_v^2(T_v+T_{Rv})(T_h+T_{Rh})\delta(f)+\frac{g}{4}G_v^2\left\{T_3^2+T_4^2\right\}H(f) \tag{B3c}$$

$$S_{w3,w3}(f)=\frac{g}{4}G_v^2T_3^2\delta(f)+\frac{g}{2}G_v^2(T_v+T_{Rv})(T_h+T_{Rh})\times H(f)+\frac{g}{8}G_v^2\left\{T_3^2-T_4^2\right\}H(f) \tag{B3d}$$

$$S_{w3,wh}(f)=\frac{\sqrt{g^3}}{2}G_v^2(T_h+T_{Rh})T_3\delta(f)+\frac{\sqrt{g^3}}{2}G_v^2(T_h+T_{Rh})T_3H(f) \tag{B3e}$$

$$S_{wh,wh}(f)=g^2G_v^2(T_h+T_{Rh})^2\delta(f)+g^2G_v^2(T_h+T_{Rh})^2H(f) \tag{B3f}$$

where the Fourier transforms of the terms modulated by either $\cos(4\pi f_c\tau)$ or $\sin(4\pi f_c\tau)$ in the expressions for autocorrelations and lag cross correlations in (B3a)–(B3f) are not included here because they will be filtered out by the subsequent low-pass filters. In (B3a)–(B3f), $g = G_h/G_v$ is the gain imbalance between V- and H-pol channels, $S_{wa,wa}(f)$ is the spectrum of $w_a(t)$, and $S_{wa,wb}(f)$ is the cross spectrum of $w_a(t)$ and $w_b(t)$. The "hat" function $H(f)$ in (B3a)–(B3f) is given by

$$\begin{cases} H(f) = \frac{1}{B}\left(1 - \left|\frac{f}{B}\right|\right) & \text{for } |f| \langle B \\ = 0 & \text{otherwise.} \end{cases} \tag{B4}$$

The power spectra and the cross spectra of the signals $x_v(t)$, $x_h(t)$, and $x_3(t)$ at the output of the low-pass filters can be found from (B3) by

$$S_{a,b}(f) = S_{wa,wb}(f) \cdot |L(f)|^2 \tag{B5}$$

where $a = v, h,$ and 3, and $L(f)$ is the transfer function of the low-pass filter, defined as zero for $|f| \geq 1/2\tau$ and one otherwise, where τ is the integration time. Near dc, the hat function $H(f)$ can be approximated by its value at $f = 0$. The power spectra at $|f| < 1/2\tau$ are given by

$$S_{v,v}(f) = G_v^2(T_v + T_{Rv})^2\delta(f) + \frac{1}{B}G_v^2(T_v + T_{Rv})^2 \tag{B6a}$$

$$S_{v,3}(f) = \frac{\sqrt{g}}{2}G_v^2(T_v + T_{Rv})T_3\delta(f) + \frac{\sqrt{g}}{2B}G_v^2(T_v + T_{Rv})T_3 \tag{B6b}$$

$$S_{v,h}(f) = gG_v^2(T_v + T_{Rv})(T_h + T_{Rh})\delta(f) + \frac{g}{4B}G_v^2\left\{T_3^2 + T_4^2\right\} \tag{B6c}$$

$$S_{3,3}(f) = \frac{g}{4}G_v^2T_3^2\delta(f) + \frac{g}{2B}G_v^2(T_v + T_{Rv})(T_h + T_{Rh}) + \frac{g}{8B}G_v^2\left\{T_3^2 - T_4^2\right\} \tag{B6d}$$

$$S_{3,h}(f) = \frac{\sqrt{g^3}}{2}G_v^2(T_h + T_{Rh})T_3\delta(f) + \frac{\sqrt{g^3}}{2B}G_v^2(T_h + T_{Rh})T_3 \tag{B6e}$$

$$S_{h,h}(f) = g^2G_v^2(T_h + T_{Rh})^2\delta(f) + \frac{g^2}{B}G_v^2(T_h + T_{Rh})^2. \tag{B6f}$$

In the above expressions, the terms on the right-hand side that involve the Dirac delta function $\delta(f)$ are the dc components of the spectra. The others are the ac components.

The power contained in the dc and ac frequency components of $x_v(t)$, $x_3(t)$, and $x_h(t)$ are obtained by integrating over the appropriate portions of their spectra. The expected value of these signals (i.e., the dc component of their spectra) is proportional to the four associated brightness temperatures. The variance of the signals (i.e., the integral over the ac component of their spectra) is due to the additive noise present in the measurements. The expected value (dc) and variance (ac) are separately given as follows:

$$R_{v,v}^{\mathrm{dc}}(0) = G_v^2(T_v + T_{Rv})^2$$

$$R_{v,v}^{\mathrm{ac}}(0) = \frac{1}{B\tau}G_v^2(T_v + T_{Rv})^2 \tag{B7a}$$

$$R_{v,3}^{\mathrm{dc}}(0) = \frac{\sqrt{g}}{2}G_v^2(T_v + T_{Rv})T_3$$

$$R_{v,3}^{\mathrm{ac}}(0) = \frac{\sqrt{g}}{2B\tau}G_v^2(T_v + T_{Rv})T_3 \tag{B7b}$$

$$R_{v,h}^{\mathrm{dc}}(0) = gG_v^2(T_v + T_{Rv})(T_h + T_{Rh})$$

$$R_{v,h}^{\mathrm{ac}}(0) = \frac{g}{4B\tau}G_v^2\left\{T_3^2 + T_4^2\right\} \tag{B7c}$$

$$R_{3,3}^{\mathrm{dc}}(0) = \frac{g}{4}G_v^2T_3^2$$

$$R_{3,3}^{\mathrm{ac}}(0) = \frac{g}{2B\tau}G_v^2(T_v + T_{Rv})(T_h + T_{Rh}) + \frac{g}{8B\tau}G_v^2\left\{T_3^2 - T_4^2\right\} \tag{B7d}$$

$$R_{3,h}^{\mathrm{dc}}(0) = \frac{\sqrt{g^3}}{2}G_v^2(T_h + T_{Rh})T_3$$

$$R_{3,h}^{\mathrm{ac}}(0) = \frac{\sqrt{g^3}}{2B\tau}G_v^2(T_h + T_{Rh})T_3 \tag{B7e}$$

$$R_{h,h}^{\mathrm{dc}}(0) = g^2G_v^2(T_h + T_{Rh})^2$$

$$R_{h,h}^{\mathrm{ac}}(0) = \frac{1}{B\tau}g^2G_h^2(T_h + T_{Rh})^2. \tag{B7f}$$

REFERENCES

[1] G. Evans and C. W. McLeish, *RF Radiometer Handbook*. Dedham, MA: Artech House, 1977.

[2] A. Ishimaru, *Electromagnetic Wave Propagation, Radiation, and Scattering*. Englewood Cliffs, NJ: Prentice-Hall, 1991.

[3] P. Gaiser, K. M. St Germain, E. M. Twarog, G. A. Poe, W. Purdy, D. Richardson, W. Grossman, W. L. Jones, D. Spencer, G. Golba, J. Cleveland, L. Choy, R. M. Bevilacqua, and P. S. Chang, "The WindSat spaceborne polarimetric microwave radiometer: Sensor description and early orbit performance," *IEEE Trans. Geosci. Remote Sens.*, vol. 42, no. 11, pp. 2347–2361, Nov. 2004.

[4] F. M. Monaldo, "Evaluation of WindSat wind vector performance with respect to QuikSCAT estimates," *IEEE Trans. Geosci. Remote Sens.*, vol. 44, no. 3, pp. 638–644, Mar. 2006.

[5] S. J. English, B. Candy, A. Jupp, D. Bebbington, S. Smith, and A. Holt, "An evaluation of the potential of polarimetric radiometry for numerical weather prediction using QuikSCAT," *IEEE Trans. Geosci. Remote Sens.*, vol. 44, no. 3, pp. 668–675, Mar. 2006.

[6] S. H. Yueh, W. J. Wilson, S. V. Nghiem, F. K. Li, and W. B. Ricketts, "Polarimetric measurements of sea surface brightness temperatures using an aircraft K-band radiometer," *IEEE Trans. Geosci. Remote Sens.*, vol. 33, no. 1, pp. 85–92, Jan. 1995.

[7] J. R. Piepmeier, "Calibration of passive microwave polarimeters that use hybrid coupler-based correlators," *IEEE Trans. Geosci. Remote Sens.*, vol. 42, no. 2, pp. 391–400, Feb. 2004.

[8] H. Suess and M. Soellner, "Fully polarimetric measurements of brightness temperature distributions with a quasi-optical radiometer system at 90 GHz," *IEEE Trans. Geosci. Remote Sens.*, vol. 43, no. 5, pp. 1170–1179, May 2005.

[9] J. L. Pawsey and R. N. Bracewell, *Radio Astronomy*. London, U.K.: Oxford Univ. Press, 1955.

[10] C. S. Ruf, "Constraints on the polarization purity of a Stokes microwave radiometer," *Radio Sci.*, vol. 33, no. 6, pp. 1617–1639, 1998.

[11] A. Colliander, L. Ruokokoski, J. Suomela, K. Veijola, J. Kettunen, V. Kangas, A. Aalto, M. Levander, H. Greus, M. T. Hallikainen, and J. Lahtinen, "Development and calibration of SMOS reference radiometer," *IEEE Trans. Geosci. Remote Sens.*, vol. 45, no. 7, pp. 1967–1977, Jul. 2007.

[12] C. S. Ruf, C. T. Swift, A. B. Tanner, and D. M. Le Vine, "Interferometric synthetic aperture microwave radiometry for the remote sensing of the earth," *IEEE Trans. Geosci. Remote Sens.*, vol. 26, no. 5, pp. 597–611, Sep. 1988.

[13] C. S. Ruf and J. Li, "A correlated noise calibration standard for interferometric, polarimetric, and autocorrelation microwave radiometers," *IEEE Trans. Geosci. Remote Sens.*, vol. 41, no. 10, pp. 2187–2196, Oct. 2003.

[14] R. De Roo, C. Ruf, B. Lim, L. van Nieuwstadt, C. Wineland, and R. Gandhi, "L-band and K-band correlated noise calibration system (CNCS) architecture," in *Proc. Spec. Meeting Microw. Radiometry*, San Juan, PR, Feb. 28–Mar. 3, 2006.

[15] B. H. Lim and C. S. Ruf, "Calibration of a fully polarimetric microwave radiometer using a digital polarimetric noise source," in *Proc. IEEE Int. Geosci. Remote Sens. Symp.*, Denver, CO, Jul. 31–Aug. 4, 2006.

Jinzheng Peng received the B.S. degree from Wuhan University, Wuhan, China, in 1991 and the M.S. degree from the University of Massachusetts, Amherst, in 2003, all in electrical engineering. He is currently working toward the Ph.D. degree at the University of Michigan, Ann Arbor.

From 1991 to 2000, he was with the Beijing Institute of Remote Sensing Equipment, Beijing, China. His research interests include system-level concept development, design, analysis, and calibration for microwave remote-sensing instruments.

Christopher S. Ruf (S'85–M'87–SM'92–F'01) received the B.A. degree in physics from Reed College, Portland, OR, in 1982, and the Ph.D. degree in electrical and computer engineering from the University of Massachusetts, Amherst, in 1987.

He was with Intel Corporation, Hughes Space and Communication, the National Aeronautics and Space Administration (NASA) Jet Propulsion Laboratory, and the Pennsylvania State University, University Park. In 2000, he was a Guest Professor with the Technical University of Denmark, Lyngby. He is currently a Professor of atmospheric, oceanic, and space sciences and electrical engineering and computer science, and Director of the Space Physics Research Laboratory, University of Michigan, Ann Arbor. He has published in the areas of microwave radiometer satellite calibration, sensor and technology development, and geophysical retrieval algorithms.

Dr. Ruf is a member of the American Geophysical Union (AGU), the American Meteorological Society (AMS), and Commission F of the Union Radio Scientifique Internationale. He has served or is serving on the editorial boards of the IEEE Geoscience and Remote Sensing Society (GRS-S) Newsletter, the AGU *Radio Science*, the IEEE TRANSACTIONS ON GEOSCIENCE AND REMOTE SENSING, and the *AMS Journal of Atmospheric and Oceanic Technology*. He was a recipient of three NASA Certificates of Recognition and four NASA Group Achievement Awards, as well as the 1997 GRS-S Transactions Prize Paper Award, the 1999 IEEE Judith A. Resnik Technical Field Award, and the 2006 Symposium Prize Paper Award from the IEEE International Geoscience and Remote Sensing Symposium.